J. Fluid Mech. (2026), *vol.* 1041, R2, doi:10.1017/jfm.2026.11944



Modelling the growth of dendrites on cold substrates

Ellen Luckins[1] **and Christophe Josserand**[2]

[1]Mathematics Institute, University of Warwick, Zeeman Building, Coventry CV4 7AL, UK

[2]Laboratoire d'Hydrodynamique (LadHyX), UMR 7646 CNRS-Ecole Polytechnique, IP Paris, 91128 Palaiseau CEDEX, France

Corresponding author: Ellen Luckins, ellen.luckins@warwick.ac.uk

(Received 1 June 2026 UTC; revised 15 July 2026 UTC; accepted 22 July 2026 UTC)

We investigate theoretically the propagation of dendrites along an undercooled solid substrate. Our approach takes into account the heat diffusion in the substrate, and the solid and liquid domains, coupled by the Stefan condition at the solid–liquid interface. Using dimensional and asymptotic analysis, we deduce a simplified model in which diffusion in the liquid and horizontally in the substrate can be neglected. We obtain a self-similar solution consisting of a half-parabolic dendrite shape propagating at constant speed. We derive a scaling law for the maximum velocity, set by the Gibbs–Thomson and kinetic effects, which is in good agreement with experimental results from the literature.

Key words: icing

1. Introduction

Freezing and melting are present in natural and industrial situations, from planet formation to glacier and sea ice dynamics (Makkonen 1987), from metallurgy to icing structures and aircraft safety (Cebeci & Kafyeke 2003). Freezing/melting is a free-boundary problem driven by coupled heat transfer and surface effects at the phase-change boundary, encoded in the famous Stefan problem (Langer 1980; Davis 2001). Free dendrites – i.e. when the solid phase grows inside an infinite undercooled liquid domain – are observed to grow at a constant speed, which increases with the undercooling. The free-dendrite velocity, as well as the dendrite-tip curvature, is selected by the interplay between the thermal diffusion in the liquid and the Stefan condition at the liquid–solid interface, leading to a solubility condition. There, both Gibbs–Thomson and kinetic effects have to be taken into account,

© The Author(s), 2026. Published by Cambridge University Press. This is an Open Access article, distributed under the terms of the Creative Commons Attribution licence (https://creativecommons.org/licenses/by/4.0/), which permits unrestricted re-use, distribution and reproduction, provided the original article is properly cited.

https://doi.org/10.1017/jfm.2026.11944 Published online by Cambridge University Press

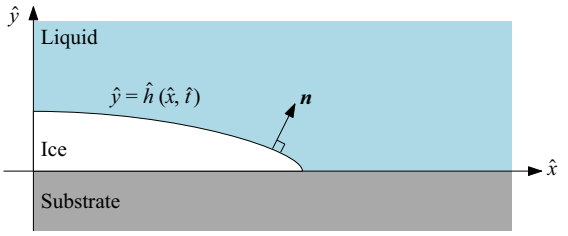


Figure 1. Schematic of an ice dendrite growing on a supercooled substrate.

as well as the anisotropy of the ice crystal, to recover the correct result, through an integro-differential equation (Ben Amar & Pomeau 1986; Kessler & Levine 1986*a*,*b*; Meiron 1986; Barbieri 1987).

Recently, similar dendrite growth has been experimentally characterised when the liquid is in contact with a cold substrate (Kong & Liu 2015; Schremb & Tropea 2016; Schremb *et al.* 2017; Grivet *et al.* 2022). There, the dendrite shape resembles a half-parabola that propagates along the substrate at a constant speed, which increases with the substrate undercooling, whether the liquid is undercooled or not. Although these dendrites therefore present similar features to the free dendrites, the driving feature is different: while heat diffusion in the liquid phase controls free-dendrite formation, diffusion into the substrate typically dominates due to its high effusivity compared with water. This manifests in particular through a much higher dendrite speed on a substrate than for free dendrites at the same undercooling, as well as through a different dependence of the dendrite speed on the undercooling. Although theoretical approaches have been proposed using strong assumptions on the dendrite shapes (Kong & Liu 2015; Schremb *et al.* 2017; Grivet *et al.* 2022), a complete understanding of the shape and velocity selection for the dendrites on substrates is still lacking. In the present paper, we propose the first theoretical model taking into account the coupling between heat diffusion and surface processes in the Stefan problem without *a priori* hypothesis on the dendrite shape and the temperature field.

2. Model statement

We consider the growth of a two-dimensional dendrite on the surface of a semi-infinite cold substrate. We will specifically consider the case of ice and water, but the model holds more generally. The three phases of interest, illustrated in figure 1, are the substrate in $\hat{y} < 0$, the growing ice dendrite in $\hat{y} \in (0, \hat{h}(\hat{x}, \hat{t}))$, and the liquid in $\hat{y} > \hat{h}(\hat{x}, \hat{t})$. (Throughout, a hat denotes a dimensional variable.)

In each phase, heat is transported by conduction. (We neglect any convective effects in the liquid, including any flows generated by expansion/contraction during freezing.) We assume that the thermal conductivity k, specific heat capacity c_p and density ρ of each phase are constant. Using superscripts s, i, l to denote substrate, ice and liquid, respectively, the heat equations for the temperature $\hat{T}$ of each phase are given by

$$\rho^s c_p^s \hat{T}^s_{\hat{t}} = k^s \, \hat{\nabla}^2 \hat{T}^s \quad \text{in} \quad \hat{y} < 0, \tag{2.1a}$$

$$\rho^i c_p^i \hat{T}^i_{\hat{t}} = k^i \, \hat{\nabla}^2 \hat{T}^i \quad \text{in} \quad 0 < \hat{y} < \hat{h}(\hat{x}, \hat{t}), \tag{2.1b}$$

$$\rho^l c_p^l \hat{T}^l_{\hat{t}} = k^l \, \hat{\nabla}^2 \hat{T}^l \quad \text{in} \quad \hat{y} > \hat{h}(\hat{x}, \hat{t}), \tag{2.1c}$$

with subscript $\hat{t}$ denoting the time derivative. At the substrate surface $\hat{y} = 0$, we prescribe continuity of temperature and of heat flux, so that

https://doi.org/10.1017/jfm.2026.11944 Published online by Cambridge University Press

$$\hat{T}^s = \begin{cases} \hat{T}^i & \text{if } \hat{h} > 0, \\ \hat{T}^l & \text{if } \hat{h} = 0, \end{cases} \quad k^s \hat{T}^s_{\hat{y}} = \begin{cases} k^i \hat{T}^i_{\hat{y}} & \text{if } \hat{h} > 0, \\ k^l \hat{T}^l_{\hat{y}} & \text{if } \hat{h} = 0, \end{cases} \quad \text{on} \quad \hat{y} = 0, \tag{2.1d}$$

with subscript $\hat{y}$ denoting the partial derivative. On the freezing interface $\hat{y} = \hat{h}(\hat{x}, \hat{t})$, we impose the freezing temperature and the Stefan boundary condition for the jump in the heat flux due to the latent heat of phase change, so that on $\hat{y} = \hat{h}(\hat{x}, \hat{t})$,

$$\hat{T}^i = \hat{T}^l = T_f \left(1 + d_\gamma \hat{\kappa}\right) - \mu \hat{V}_n, \quad \rho^i \mathcal{L} \hat{V}_n = k^i \, \hat{\boldsymbol{\nabla}} \hat{T}^i \cdot \boldsymbol{n} - k^l \, \hat{\boldsymbol{\nabla}} \hat{T}^l \cdot \boldsymbol{n}. \tag{2.1e}$$

Here, $\mathcal{L}$ is the latent heat of fusion, and $\boldsymbol{n}$, $\hat{V}_n$ and $\hat{\kappa}$ are the interface unit normal, normal velocity and curvature, given by

$$\boldsymbol{n} = \frac{1}{\left(1 + \hat{h}_{\hat{x}}^2\right)^{1/2}} \begin{pmatrix} -\hat{h}_{\hat{x}} \\ 1 \end{pmatrix}, \quad \hat{V}_n = \frac{\hat{h}_{\hat{t}}}{\left(1 + \hat{h}_{\hat{x}}^2\right)^{1/2}}, \quad \hat{\kappa} = \frac{\hat{h}_{\hat{x}\hat{x}}}{\left(1 + \hat{h}_{\hat{x}}^2\right)^{3/2}} \tag{2.2}$$

for our chosen geometry, and T_f is the equilibrium freezing temperature of a flat interface. The second term in the first equation of (2.1*e*), $T_f d_\gamma \hat{\kappa}$, is the Gibbs–Thomson effect, whereby the freezing temperature is reduced at high curvatures (note $\hat{\kappa} < 0$), with $d_\gamma = \gamma_{li}/\rho^i \mathcal{L}$ denoting the thermo-capillary length, where $\gamma_{li} \approx 3 \times 10^{-2}$ J m^{-2} is the liquid–ice surface tension. The final term in the first equation of (2.1*e*), $-\mu \hat{V}_n$, captures the kinetic effect on the interface temperature, with μ the inverse kinetic rate parameter: the freezing rate is reduced at lower temperatures. For simplicity, we assume a linear kinetic effect; other nonlinear relations between $\hat{V}_n$ and the interface undercooling are relevant at larger undercoolings (Shibkov *et al.* 2005).

Initially, the substrate is at uniform temperature $T_* < T_f$. To close the model, we also require an initial condition for the liquid (e.g. another constant) and the initial shape of the dendrite; we will later make a systematic reduction and find that our reduced model does not depend on the initial liquid temperature, nor does it require an initial dendrite shape.

2.1. *Non-dimensionalisation*

We non-dimensionalise the model by making the rescalings

$$(\hat{x}, \hat{y}) = [h](x, y), \quad \hat{h} = [h]h, \quad \hat{t} = \frac{\rho^i \mathcal{L}[h]^2}{k^i \, \Delta T} t, \quad \hat{T} = T_* + \Delta T T. \tag{2.3}$$

The interface velocity V_n and curvature κ are also non-dimensionalised with these length and time scales. It is not clear *a priori* what determines the length scale of the height of the dendrite. We use an arbitrary length scale $[h]$, and will see that the choice of $[h]$ does not affect the predictions of our reduced model.

The temperature variation is set by the substrate supercooling as $\Delta T = T_f - T_*$. The Stefan number, which is the ratio of sensible heat to latent heat, is therefore

$$St = \frac{c_p^i \, \Delta T}{\mathcal{L}} \approx 6 \times 10^{-3} – 6 \times 10^{-2} \tag{2.4}$$

(estimated using data listed below) and is typically small. Thus the freezing rate is limited by heat conduction, justifying our choice of the time scale in (2.3), which balances the Stefan boundary condition.

https://doi.org/10.1017/jfm.2026.11944 Published online by Cambridge University Press

Using the scalings in (2.3), the dimensionless model is

$$\frac{r^s}{K^s}\,St\,T_t^s = \nabla^2 T^s \qquad \text{in} \quad y<0, \tag{2.5a}$$

$$St\,T_t^i = \nabla^2 T^i \qquad \text{in} \quad 0<y<h, \tag{2.5b}$$

$$\frac{r^l}{K^l}\,St\,T_t^l = \nabla^2 T^l \qquad \text{in} \quad y>h, \tag{2.5c}$$

$$T^i = T^l = 1+\gamma\kappa-\lambda V_n \qquad \text{on} \quad y=h, \tag{2.5d}$$

$$V_n = \boldsymbol{\nabla} T^i\cdot\boldsymbol{n} - K^l\,\boldsymbol{\nabla} T^l\cdot\boldsymbol{n} \qquad \text{on} \quad y=h, \tag{2.5e}$$

$$T^s = \begin{cases} T^i & \text{if } h>0,\\ T^l & \text{if } h=0,\end{cases} \qquad K^s T_y^s = \begin{cases} T_y^i & \text{if } h>0,\\ K^l T_y^l & \text{if } h=0,\end{cases} \qquad \text{on} \quad y=0, \tag{2.5f}$$

with the far-field substrate temperature $T^s\to 0$. Here, we have introduced several dimensionless groups in addition to the Stefan number (2.4), defined by

$$r^l = \frac{c_p^l\rho^l}{c_p^i\rho^i}\approx 2, \quad r^s = \frac{c_p^s\rho^s}{c_p^i\rho^i}\approx 2, \quad K^l = \frac{k^l}{k^i}\approx 0.3, \quad K^s = \frac{k^s}{k^i}\approx 20, \tag{2.6a}$$

$$\gamma = \frac{d_\gamma T_f}{\Delta T\,[h]}\approx 3\times 10^{-4}{-}3\times 10^{-3}, \quad \lambda = \frac{\mu k^i}{\rho^i\mathcal{L}[h]}\approx (1{-}5)\times 10^{-2}. \tag{2.6b}$$

The groups r^l, r^s, K^l, K^s quantify the relative thermal properties of the different materials, while γ and λ quantify the magnitude of the Gibbs–Thomson and kinetic effects on the ice growth, relative to the heat transfer processes.

The dimensionless group estimates are computed using the well-known dimensional values $c_p^i = 2\times 10^3$ J kg^{-1} K^{-1}, $c_p^l = 4\times 10^3$ J kg^{-1} K^{-1}, $\rho^i = 9\times 10^2$ kg m^{-3}, $\rho^l = 10^3$ kg m^{-3}, $k^i = 2.2$ W m^{-1} K^{-1}, $k^l = 0.6$ W m^{-1} K^{-1}, $T_f = 273$ K, $\mathcal{L} = 3.3\times 10^5$ J kg^{-1}, $d_\gamma = 10^{-10}$ m, $c_p^s = 8\times 10^2$ J kg^{-1} K^{-1}, $k^s = 4\times 10$ W m^{-1}K^{-1}, $\rho^s = 4\times 10^3$ kg m^{-3}, $\Delta T = 1{-}10$ K and $[h] = 10^{-5}$ m, for a sapphire substrate (Grivet *et al.* 2022), and $[h]$ measurements of Kong & Liu (2015).

There is no accepted value for the inverse kinetic rate parameter μ, as discussed by both Xu *et al.* (2016) and Wang *et al.* (2019). Wang *et al.* (2019) fit measurements of free-dendrite growth rate in supercooled water to a Wilson–Frenkel model for the freezing kinetics, which is nonlinear in ΔT. Linearising their fit for relatively small supercoolings ΔT, we find $\mu\approx 13$ K s m^{-1}. Xu *et al.* (2016) use laser-pulsed heating to carefully control ice growth to quantify the kinetic growth rate. Their experimental measurements are also fitted to a Wilson–Frenkel model; on linearisation, we find $\mu\approx 69$ K s m^{-1}. These two values indicate the order of magnitude that we should expect of μ, but also highlight the uncertainty, with significant variation in results across the literature.

All of r^l, r^s, K^l are of order 1. For the conductive sapphire substrate, K^s is large, so we will study the case $K^s\gg 1$. As above, we expect $St\ll 1$, except at extreme supercoolings ΔT. We have γ, $\lambda\ll 1$, indicating that the freezing is limited by heat transfer, rather than the Gibbs–Thomson or freezing kinetics. However, we will later see that either or both of these effects can become significant near the dendrite tip, and are important in setting the dendrite growth velocity.

https://doi.org/10.1017/jfm.2026.11944 Published online by Cambridge University Press

3. Model reduction and travelling-wave solution

We non-dimensionalised with the height $[h]$ of the dendrite, but the vertical diffusion length scales in the substrate and liquid are different. We thus rescale

$$y = \sqrt{\frac{K^s}{r^s\,St}}\,Y \text{ in the substrate}, \quad y = \sqrt{\frac{K^l}{r^l\,St}}\,\mathcal{Y} \text{ in the liquid}. \tag{3.1}$$

We note that our assumption of an infinite-depth substrate breaks down if the substrate diffusion length scale is comparable to the substrate depth; we require substrate depths much larger than $[h]\sqrt{K^s/(r^s\,St)} \approx 4 \times 10^{-4}$ m using the data in § 2.1.

Experimentally, ice dendrites on substrates are seen to grow at a constant speed (Kong & Liu 2015; Grivet *et al.* 2022). We therefore look for a travelling-wave solution of our model, by making the change of variables

$$x = V(t + X) \quad \text{and} \quad h(x, t) = H(X). \tag{3.2}$$

Here, V is the (constant) speed at which the dendrite propagates to the right. The horizontal length scale must also be V, to retain the balance in the Stefan boundary condition (2.5*e*). We fix $H = 0$ at $X = 0$. Making both the rescalings (3.1) and the travelling-wave ansatz (3.2), and looking for a steady solution (dependent only on X, not t), the dimensionless model becomes

$$-T^s_X = \frac{1}{V^2}\frac{K^s}{r^s St}T^s_{XX} + T^s_{YY} \quad \text{in} \quad Y < 0, \tag{3.3a}$$

$$-StT^i_X = \frac{1}{V^2}T^i_{XX} + T^i_{yy} \quad \text{in} \quad 0 < y < H(X), \tag{3.3b}$$

$$-T^l_X = \frac{1}{V^2}\frac{K^l}{r^l St}T^l_{XX} + T^l_{\mathcal{Y}\mathcal{Y}} \quad \text{in} \quad \mathcal{Y} > \sqrt{\frac{r^l St}{K^l}}\,H(X), \tag{3.3c}$$

with, on $y = H(X)$,

$$T^i = T^l = 1 + \frac{\gamma}{V^2}\frac{H_{XX}}{(1 + H_X^2/V^2)^{3/2}} + \lambda\frac{H_X}{(1 + H_X^2/V^2)^{1/2}}, \tag{3.3d}$$

$$-H_X = T^i_y - \frac{1}{V^2}H_X T^i_X - K^l\left(\sqrt{\frac{r^l St}{K^l}}\,T^l_{\mathcal{Y}} - \frac{1}{V^2}H_X T^l_X\right), \tag{3.3e}$$

and on $y = Y = \mathcal{Y} = 0$,

$$T^s = \begin{cases} T^i & \text{if } X < 0, \\ T^l & \text{if } X > 0, \end{cases} \quad \sqrt{r^s K^s St}\,T^s_Y = \begin{cases} T^i_y & \text{if } X < 0, \\ \sqrt{r^l K^l St}\,T^l_{\mathcal{Y}} & \text{if } X > 0. \end{cases} \tag{3.3f}$$

As $Y \to -\infty$, $T^s \to 0$.

As in § 2.1, we assume $St, \gamma, \lambda \ll 1$, $r^l, r^s, K^l = O(1)$ and $K^s \gg 1$. We also assume that V is large, so that the dendrite is long and thin, as observed experimentally (Kong & Liu 2015; Grivet *et al.* 2022). Specifically, we require

$$V \gg \sqrt{K^s/(r^s St)}. \tag{3.4}$$

We define the group

$$\alpha = \sqrt{r^s K^s St} \approx 0.5\text{–}1.5 \tag{3.5}$$

https://doi.org/10.1017/jfm.2026.11944 Published online by Cambridge University Press

(using the data in § 2.1), which appears in (3.3*f*). Since $St \ll 1$ and $K^s \gg 1$, we take $\alpha = O(1)$, and later take small/large-α sublimits. Since α is proportional to both the substrate thermal effusivity $\varepsilon^s = (c_p^s \rho^s k^s)^{1/2}$ and $(\Delta T)^{1/2}$ (via St), it quantifies both the substrate's ability to remove heat, and its supercooling.

With the above assumptions, the model in the ice and substrate simplifies at leading order to

$$-T_X^s = T_{YY}^s \text{ for } Y < 0, \quad T_{yy}^i = 0 \quad \text{for} \quad 0 < y < H(X), \tag{3.6a}$$

$$T^i = 1, \quad -H_X = T_y^i \quad \text{on} \quad y = H(X), \tag{3.6b}$$

$$T^s = T^i, \quad \alpha T_Y^s = T_y^i \quad \text{on} \quad y = Y = 0, \tag{3.6c}$$

for $X < 0$, with $T^s \to 0$ as $Y \to -\infty$. In this regime, the liquid fully decouples from these equations for the ice and substrate, with negligible heat transfer into the liquid in (3.3*e*) and (3.3*f*), since $St \ll 1$ and $K^s \gg 1$. The liquid temperature could subsequently be found from (3.3*c*), but in this parameter regime, heat transfer into the liquid does not affect the leading-order dendrite growth described by (3.6). In particular, $T^s = 0$ for $X > 0$. This is the key difference from the free-dendrite problem: there, the freezing process is governed by heat diffusion into the supercooled water; here, it is governed by diffusion into the substrate.

As an aside, we note that the reverse problem of a dendrite melting due to heat diffusion into a substrate is ill-posed, since the time-like variable in the parabolic equation changes sign, and since physically this corresponds to superheated ice. Thus our model does not capture such melting scenarios.

We solve the reduced model (3.6) analytically as follows. The ice temperature T^i is linear in y, and using both boundary conditions at $y = H(X)$, it is given by $T^i(X, y) = 1 + H_X(X)(H(X) - y)$. The remaining problem for T^s and H is parabolic (viewing $-X$ as the time-like variable), admitting the similarity solution

$$T^s(X, Y) = \frac{\xi}{\alpha}\sqrt{\frac{\pi}{4}}\,\operatorname{erfc}\left(\frac{-Y}{2\sqrt{-X}}\right), \quad H(X) = \xi\sqrt{-X} \quad \text{for} \quad X < 0, \tag{3.7a}$$

where the constant ξ (monotonically increasing in α from zero to $\sqrt{2}$) is given by

$$\xi = \frac{1}{\alpha}\left(\sqrt{2\alpha^2 + \frac{\pi}{4}} - \sqrt{\frac{\pi}{4}}\right). \tag{3.7b}$$

Using the expression for $H(X)$, the ice temperature is therefore

$$T^i(X, y) = 1 - \frac{\xi}{2\sqrt{-X}}\left(\xi\sqrt{-X} - y\right). \tag{3.7c}$$

This travelling-wave solution (3.7) is shown in figure 2 for three different values, $\alpha = 0.3$, 1 and 3. In figure 2(*a*), we see that the dendrite thickness increases with α. The temperature profiles in the ice and substrate are shown in figure 2(*b*) at two locations X for different α: for fixed α, the temperature along the ice–substrate interface is constant, $T^i = T^s = 1 - \xi^2/2$. In the thinner ice near the tip, the temperature gradient is steeper in both phases. As α increases, the interface temperature decreases, with temperature gradients steeper in the ice and shallower in the substrate. In the original coordinates, the dendrite shape is

$$h(x, t) = H(x/V - t) = \xi\sqrt{t - x/V}, \tag{3.8}$$

corresponding to a (half-)parabola that translates at constant speed with time. We note that the model reduction imposes a 90° contact angle at the dendrite tip, since the temperature

https://doi.org/10.1017/jfm.2026.11944 Published online by Cambridge University Press

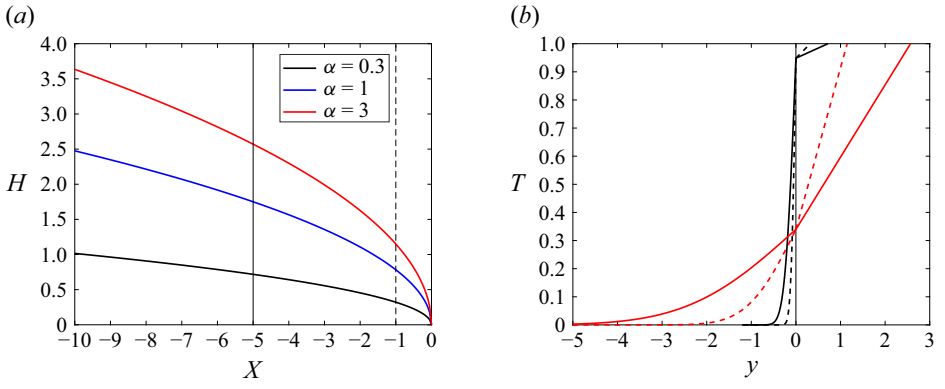


Figure 2. Travelling-wave solution (3.7). (*a*) Plot of $H(X)$ for $\alpha = 0.3$, 1 and 3. (*b*) Plot of $T^s(y)$ ($y < 0$) and $T^i(y)$ ($0 < y < H(X)$), shown at $X = -5$ (solid) and $X = -1$ (dashed), for $\alpha = 0.3$, 3 (as in the legend in (*a*)). For illustration, $K^s = 5$.

gradient in the ice becomes infinite there. More detailed analysis of the heat conduction at the dendrite tip, where horizontal conduction may be non-negligible, might result in a different contact angle.

4. What sets the dendrite velocity?

Our asymptotic travelling-wave solution is valid for any dendrite velocity V that is sufficiently large in the sense of (3.4). Both the (half-)parabolic shape of the dendrite and the infinite family of solutions (for any large speed V) are reminiscent of the infinite family of parabolic solutions in the classical case of free dendrites (Ivantsov 1947). Also like free dendrites, the thickness of the dendrite on the substrate scales inversely with speed, with aspect ratio $y/X \sim 1/V$.

However, both the kinetic and Gibbs–Thomson effects (neglected in the travelling-wave solution) become important for large V, and either could limit the dendrite velocity, depending on which becomes significant at the lower speed V. Quantitatively, the parabolic solution $H = \xi\sqrt{-X}$ approaches a maximum curvature $2V/\xi^2$ at the dendrite tip, where the normal interface velocity is also maximised, equal to V. In (3.3*d*), the dendrite tip temperature thus satisfies

$$T^i \to 1 - 2\gamma V/\xi^2 - \lambda V \quad \text{as } X \to 0. \tag{4.1}$$

It was therefore reasonable to neglect the Gibbs–Thomson term in our analysis only for sufficiently small $V \ll \xi^2/2\gamma$, and to neglect the kinetic term only for $V \ll 1/\lambda$. Rearranging (4.1), we can relate the dendrite velocity to the tip temperature by

$$V = \frac{1 - T^i|_{X=0}}{\lambda + (2\gamma/\xi^2)}. \tag{4.2}$$

As with free dendrites, we expect the growth velocity observed experimentally to be the fastest possible, since this mode will overtake all others. Thus we may view (4.2) as an estimate for the dendrite velocity.

We note that in our reduced parabolic model, the tip temperature $T^i|_{X=0}$ is not defined: the liquid–ice interface temperature is the equilibrium melting temperature, while the substrate–ice temperature at the tip is $1 - \xi^2/2$ from (3.7*c*). Our reduced model breaks down very close to the tip, where additional effects such as horizontal diffusion become non-negligible. To estimate V, we note that the coldest the freezing interface at the

https://doi.org/10.1017/jfm.2026.11944 Published online by Cambridge University Press

dendrite tip could be is the initial supercooled substrate temperature $T^i = 0$. Using this value in (4.2) gives an upper bound on the dendrite velocity V, namely

$$V^{max} = \frac{1}{\lambda + (2\gamma/\xi^2)}. \tag{4.3}$$

In reality, it is likely that $T^i > 0$ at the tip, due to heat conduction through the substrate and/or liquid ahead of the growing dendrite, reducing V below V^{max}.

We note that V^{max} is a harmonic average of the growth rate set solely by kinetic effects ($V_K = \lambda^{-1}$) and that set solely by Gibbs–Thomson effects ($V_{GT} = \xi^2/2\gamma$). Additionally, V^{max} is of order λ^{-1} or γ^{-1}, whichever is smaller; since $\lambda, \gamma \ll 1$, this justifies *a posteriori* the assumption $V \gg 1$ made in § 3.

Redimensionalising, we find that the dimensional upper bound on the dendrite speed is

$$\hat{V}^{max} = \frac{[h]}{[t]} V^{max} = \left(\frac{\mu}{\Delta T} + \frac{2T_f \gamma_{li}}{\xi^2 k^i (\Delta T)^2} \right)^{-1}. \tag{4.4}$$

This velocity $\hat{V}^{max}$ is independent of the length scale $[h]$ of the dendrite, reflecting the self-similarity of the travelling-wave solution, and reinforcing our assumption (informed by the experimental literature) of constant dendrite speed: $\hat{V}^{max}$ does not depend on $[h]$, or equivalently, on the time for which it has been growing.

4.1. *Effect of the substrate supercooling and material properties*

Similarly to free dendrites (Shibkov *et al.* 2005), we see that a different process limits the dendrite velocity (4.4), depending on the supercooling ΔT, with

$$\hat{V}^{max} \sim \begin{cases} \dfrac{\xi^2 k^i (\Delta T)^2}{2T_f \gamma_{li}} = \hat{V}_{GT} & \text{as } \Delta T \to 0, \\ \mu^{-1} \Delta T = \hat{V}_K & \text{as } \Delta T \to \infty, \end{cases} \tag{4.5}$$

so that the dendrite velocity is limited by the Gibbs–Thomson effect at small ΔT, and by the kinetic effect at high ΔT. The transition occurs near a critical supercooling, ΔT_{crit}, set by $\hat{V}_K = \hat{V}_{GT}$. Rearranging, ΔT_{crit} satisfies

$$\xi^2 \Delta T_{crit} = 2T_f \gamma_{li} / (\mu k^i), \tag{4.6}$$

where we emphasise that ξ depends on ΔT_{crit} via the Stefan number. The right-hand side of (4.6) is set by the intrinsic properties of water and ice. The left-hand side combines the supercooling ΔT and the substrate thermal properties via ξ: since ξ increases with substrate thermal effusivity ε^s, for a higher-effusivity substrate, the kinetic effects will become important at lower supercoolings.

For a sapphire substrate, we compute $\Delta T_{crit} = 0.3$ K. Properties of brass, steel and copper are given in Kong & Liu (2015), for which we find $\Delta T_{crit} \in (0.08, 0.23)$ K. These critical supercooling values are an order of magnitude smaller than for free dendrites, found to be 4 K by Shibkov *et al.* (2005). Faster heat conduction into the substrates than into water enables faster dendrite growth, so that kinetic effects limit the dendrite speed at smaller supercoolings than for free dendrites.

In figure 3(*a*), we plot $\hat{V}^{max}$ against the supercooling ΔT, for three values of the substrate effusivity ε^s. At large supercoolings, the velocity bound is set by the kinetic effect, thus independent of the substrate properties. At small supercoolings, thus low values of $\alpha \propto \sqrt{\Delta T}$, we note that ξ (given by (3.7*b*)) behaves as $\xi(\alpha) = 2\alpha/\sqrt{\pi} + O(\alpha^3)$.

https://doi.org/10.1017/jfm.2026.11944 Published online by Cambridge University Press

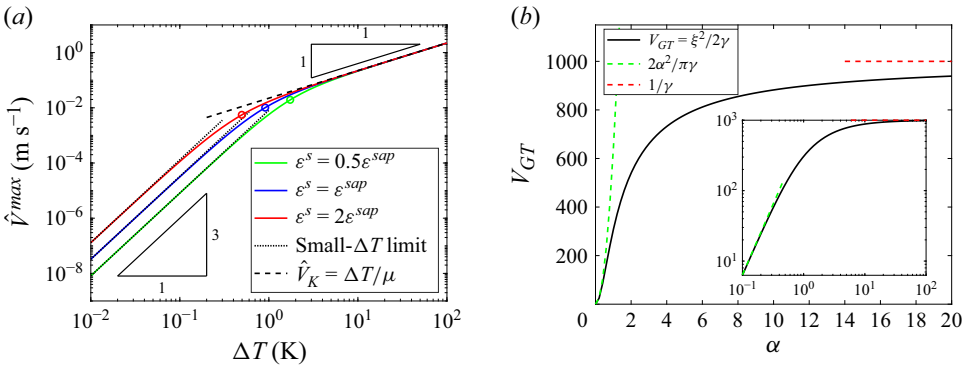


Figure 3. (*a*) Dimensional velocity prediction $\hat{V}^{max}$ variation with ΔT, for a sapphire substrate (ε^{sap}) and for double/half the effusivity. The small-ΔT limit is (4.7), and circles mark ΔT_{crit} given by (4.6). (*b*) Dimensionless dendrite velocity due solely to Gibbs–Thomson effects, $V_{GT} = \xi^2/2\gamma$, as a function of $\alpha = \sqrt{r^s K^s St} \propto \varepsilon^s$. Inset shows log-scale. Here, $\gamma = 10^{-3}$.

Using this limiting behaviour in (4.5), $\hat{V}^{max}$ is cubic in ΔT, with

$$\hat{V}^{max} \sim \frac{2(\varepsilon^s)^2}{\pi \rho^i \mathcal{L} \gamma_{li} T_f} (\Delta T)^3 \quad \text{as} \quad \Delta T \to 0. \tag{4.7}$$

The substrate material properties only affect the dendrite velocity bound $\hat{V}^{max}$ via the Gibbs–Thomson term, thus only for small $\Delta T \ll \Delta T_{crit}$. In figure 3(*b*), we show V_{GT} as a function of $\alpha = \sqrt{r^s K^s St} \propto \varepsilon^s$. For large α (high substrate effusivity), $\xi \to \sqrt{2}$. Thus $V_{GT} = \gamma^{-1}(1 + O(\alpha^{-1}))$ approaches a constant. In this large-α limit, the similarity solution (3.7) approaches

$$T^s = 0, \quad H = \sqrt{-2X}, \quad T^i = y/\sqrt{-2X}, \tag{4.8}$$

with instantaneous substrate diffusion, so the dendrite speed is solely limited by the Gibbs–Thomson effect. Conversely, for low substrate effusivity, $\alpha \to 0$, the dendrite velocity is $V_{GT} \sim 2\alpha^2/\pi\gamma + O(\alpha^4/\gamma)$, so that heat transfer into the substrate also limits the dendrite velocity.

4.2. *Comparison with experiment*

We compare our scaling law $\hat{V}^{max}$ with experimental data from the literature in figure 4. We note that there are discrepancies between the results of different experimental groups, perhaps due to slightly differing substrate properties, or to the differing geometries: Schremb *et al.* (2017) study growth of a dendrite in a Hele-Shaw cell, while Kong & Liu (2015) consider a three-dimensional axisymmetric dendrite, and Grivet *et al.* (2022) the propagation of a crystal when a droplet spreads on a substrate. All of the data are for $\Delta T > \Delta T_{crit}$, so that $\hat{V}^{max} \approx \mu^{-1}\Delta T$, independent of substrate, for the majority of the ΔT range. Experimental verification of the Gibbs–Thomson limited regime for $\Delta T < \Delta T_{crit}$ would require experiments at very low supercoolings. To fit the data, we take $\mu = 45\ \mathrm{K\,s\,m^{-1}}$, within the range discussed in § 2.1, showing this full range by the grey shaded region. Although μ is not well known, the range captures the experimental data. Moreover, the Gibbs–Thomson effect alone certainly does not limit the dendrite speed: we also show $\hat{V}_{GT}$ ($\propto \Delta T^2$ as $\Delta T \to \infty$) (dashed lines), which is inconsistent with the observed scaling and a significant overestimate of the experimental data. This indicates

https://doi.org/10.1017/jfm.2026.11944 Published online by Cambridge University Press

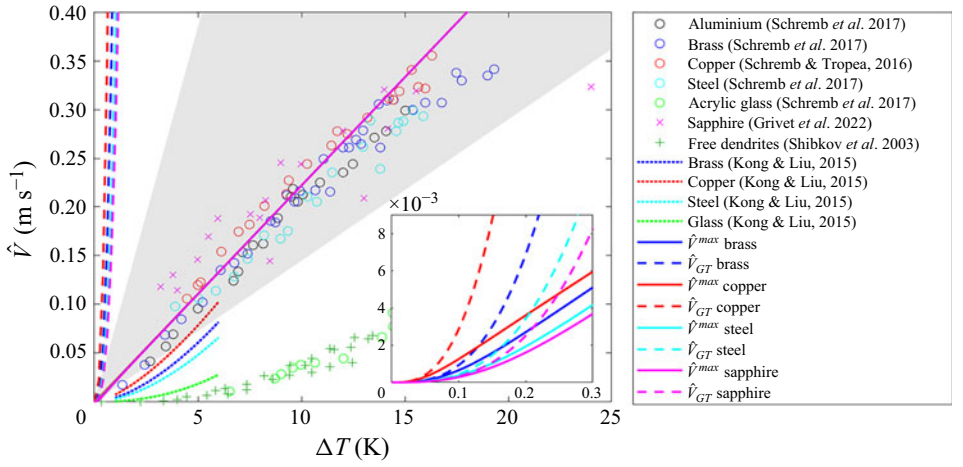


Figure 4. The maximum dendrite velocity $\hat{V}^{max}$ given by (4.4) (solid lines), along with $\hat{V}_{GT}$ from (4.5) (dashed lines) compared with experimental data from the literature (symbols and dotted lines). The inset shows behaviour near the origin. We use the data in § 2.1, taking $\mu = 45\,\mathrm{K\,s\,m^{-1}}$, and show the range $\mu \in (13, 69)\,\mathrm{K\,s\,m^{-1}}$ estimated in § 2.1 as the grey shaded area. Additional substrate properties (k^s, c_p^s, ρ^s for steel, brass, copper) are taken from Kong & Liu (2015).

that kinetic effects are the important limiting factor for the range of experimental values shown.

We also show velocity data for a glass substrate, which is similar to free dendrites (Shibkov *et al.* 2003). Since $K^s = 0.3$ is not large, our theory is invalid: liquid conduction dominates the substrate for glass.

The experimental data show a slight substrate dependence not captured by $\hat{V}^{max}$: dendrites grow faster on copper than on steel. The correct trend is seen in $\hat{V}^{max}$ at low ΔT, indicating that α, or substrate effusivity, is the correct parameter to capture substrate dependence. To understand substrate dependence in the kinetic-limited regime, we would need to consider more carefully the processes near the dendrite tip, where horizontal diffusion in the substrate becomes important (on a length scale $X \sim K^s/(r^s\,St\,V^2) \sim \lambda^2 K^s/(r^s\,St)$, balancing (3.3*a*) when $V \sim \lambda^{-1}$). We anticipate that a detailed analysis of the heat-conduction boundary layer at the dendrite tip might result in a small correction to the tip temperature from the initial supercooling $T^i = 0$ used to derive V^{max}, which could account for the small substrate dependence in the velocity. Heat transfer between the substrate and liquid ahead of the dendrite could also be important, although this may be inconsistent with the travelling-wave ansatz, as the liquid temperature would evolve over time.

4.3. *Dendrite tip curvature*

Using (4.3), we estimate the dimensional dendrite-tip radius of curvature to be

$$\hat{R} = \frac{1}{|\hat{\kappa}|} = \frac{\xi^2[h]}{2V^{max}} = [h]\left(\gamma + \frac{\lambda\xi^2}{2}\right) = \frac{d_\gamma T_f}{\Delta T} + \frac{\xi^2 \mu k^i}{2\rho^i \mathcal{L}}. \tag{4.9}$$

For $\Delta T \ll \Delta T_{crit}$, when the dendrite is Gibbs–Thomson limited, the Gibbs–Thomson term $d_\gamma T_f/\Delta T$ in (4.9) dominates, so that $\hat{R}$ is independent of the substrate properties, and proportional to ΔT^{-1}, similar to the free-dendrite case (Tirmizi & Gill 1987, figure 5). For $\Delta T \gg \Delta T_{crit}$, kinetic effects determine $\hat{V}^{max}$ and $\hat{R}$, with substrate dependence

https://doi.org/10.1017/jfm.2026.11944 Published online by Cambridge University Press

via ξ. As $\xi \to \sqrt{2}$ for large ΔT, $\hat{R} \to 3 \times 10^{-7}$ m becomes constant. This agrees with the experiments of Schremb *et al.* (2017), who observe little variation of $\hat{R}$ with the supercooling or substrate, fitting $\hat{R} \in (3.29, 3.74) \times 10^{-7}$ m, for their various substrate materials.

5. Conclusion

We have developed an analytical model for ice dendrite growth on an undercooled substrate. At first approximation, we showed that the heat diffusion in the substrate governs the dynamics, with negligible diffusion in the water. We demonstrate that in this framework, the dendrite is a half-parabola propagating at constant velocity along the substrate. We also argue that for most cases, the kinetic effect controls this velocity, with a linear dependence of velocity with the undercooling, in good agreement with former experiments. A more complete approach would require accounting for lateral heat diffusion in the substrate, and the influence of the liquid, likely requiring numerical simulations.

Funding. E.K.L. is grateful for support from the Leverhulme Trust through an Early Career Fellowship ECF-2024-172. This work was partially supported (C.J.) by Agence de l'Innovation de Défense via Centre Interdisciplinaire d'Etudes pour la Défense et la Sécurité (project 2021 - ICING).

Declaration of interests. The authors report no conflict of interest.

References

Barbieri, A. 1987 Velocity selection at large undercooling in a two-dimensional nonlocal model of solidification. *Phys. Rev. A* **36**, 5353–5358.

Ben Amar, M. & Pomeau, Y. 1986 Theory of dendritic growth in a weakly undercooled melt. *Europhys. Lett.* **2** (4), 307–314.

Cebeci, T. & Kafyeke, F. 2003 Aircraft icing. *Annu. Rev. Fluid Mech.* **35**, 11–21.

Davis, S.H. 2001 *Solidification*. Cambridge University Press.

Grivet, R., Monier, A., Huerre, A., Josserand, C. & Séon, T. 2022 Contact line catch up by growing ice crystals. *Phys. Rev. Lett.* **128** (25), 254501.

Ivantsov, G.P. 1947 Temperature field around a spherical, cylindrical and needle-shaped crystal, growing in a supercooled melt. *Dokl. Akad. Nauk SSSR* **58**, 567.

Kessler, D.A. & Levine, H. 1986*a* Stability of dendritic crystals. *Phys. Rev. Lett.* **57**, 3069–3072.

Kessler, D.A. & Levine, H. 1986*b* Velocity selection in dendritic growth. *Phys. Rev. B* **33**, 7867(R)–7870(R).

Kong, W. & Liu, H. 2015 A theory on the icing evolution of supercooled water near solid substrate. *Intl J. Heat Mass Transfer* **91**, 1217–1236.

Langer, J. 1980 Instabilities and pattern formation in crystal growth. *Rev. Mod. Phys.* **52**, 1–28.

Makkonen, L. 1987 Salinity and growth rate of ice formed by sea spray. *Cold Reg. Sci. Technol.* **14**, 163–171.

Meiron, D.I. 1986 Selection of steady states in the two-dimensional symmetric model of dendritic growth. *Phys. Rev. A* **33**, 2704–2715.

Schremb, M., Campbell, J.M., Christenson, H.K. & Tropea, C. 2017 Ice layer spreading along a solid substrate during solidification of supercooled water: experiments and modeling. *Langmuir* **33** (19), 4870–4877.

Schremb, M. & Tropea, C. 2016 Solidification of supercooled water in the vicinity of a solid wall. *Phys. Rev. E* **94** (5), 052804.

Shibkov, A.A., Golovin, Y.I., Zheltov, M.A., Korolev, A.A. & Leonov, A.A. 2003 Morphology diagram of nonequilibrium patterns of ice crystals growing in supercooled water. *Phys. A: Stat. Mech. Applics* **319**, 65–79.

Shibkov, A.A., Zheltov, M.A., Korolev, A.A., Kazakov, A.A. & Leonov, A.A. 2005 Crossover from diffusion-limited to kinetics-limited growth of ice crystals. *J. Cryst. Growth* **285** (1–2), 215–227.

https://doi.org/10.1017/jfm.2026.11944 Published online by Cambridge University Press

TIRMIZI, S.H. & GILL, W.N. 1987 Effect of natural convection on growth velocity and morphology of dendritic ice crystals. *J. Cryst. Growth* **85** (3), 488–502.

WANG, T., LÜ, Y., AI, L., ZHOU, Y. & CHEN, M. 2019 Dendritic growth model involving interface kinetics for supercooled water. *Langmuir* **35** (15), 5162–5167.

XU, Y., PETRIK, N.G., SMITH, R.S., KAY, B.D. & KIMMEL, G.A. 2016 Growth rate of crystalline ice and the diffusivity of supercooled water from 126 to 262 K. *Proc. Natl Acad. Sci. USA* **113** (52), 14921–14925.

https://doi.org/10.1017/jfm.2026.11944 Published online by Cambridge University Press